Stress-Induced Crystallization around a Crack Tip in Natural Rubber

S. Trabelsi, P.-A. Albouy, and J. Rault*

Laboratoire de Physique des Solides, UMR 8502,Université de Paris-Sud, Bât. 510, 91405 Orsay, France

Received July 15, 2002

ABSTRACT: Stress-induced crystallization, orientation, and crystallinity have been measured by X-ray diffraction around cracks in a *cis*-1,4-polyisoprene sample drawn at low ratio, $\lambda < 3.5$. A zone of maximum crystallinity and a transition zone of varying crystallinity are observed; the dimensions of these semicrystalline zones surrounding the crack tip are measured as a function of the draw ratio, crack length, and cross-link density. An isocrystallinity map is established; this permits one to measure the local draw ratio and then the local stress around the crack tip. The stress distribution around the crack tip is compared with the scaling laws predicted by the linear or nonlinear elasticity theories. Finally, one shows the existence of a relaxed zone between the crack tip, the crack surface, and the lateral sides of the sample. The surface of this zone is comparable to the area of the semicrystalline zone around the crack tip and to the crack opening surface.

1. Introduction

Quite generally, it is well-known that tearing in a sample subjected to a macroscopic stress is initiated at the tip of naturally occurring flaws where local stresses are magnified.[1−5] In the case of an elastic material obeying Hook's law, the stress components $\sigma_{i,j}(r,\theta)$ around a crack tip (in polar coordinates r,θ) are given by the Inglis, Irwin, and Westergaard relation:[2] $\sigma_{i,j} = K/(\pi r)^{1/2} f_{i,j}(\theta)$ where $K = \sigma_0(2\pi a)^{1/2}$ is the stress intensity factor dependent on the crack length a, and the applied stress σ_0. The functions $f_{i,j}(\theta)$ are dependent on the polar angle and on the exact type of deformation. In amorphous polymers and elastomers, at low deformation and at large distances r from the crack tip, the stress distribution is well explained by this linear theory.[1] In the vicinity of the crack tip, finite deformations and large geometry changes arise and the material is consequently nonlinear. In this case different models give the nonlinear asymptotic solution of the stress and strain tensors around the crack tip.[2−5]

Glassy polymers and crystallizable elastomers show large differences concerning the shape of the crack during deformation; this difference illustrated in Figure 1 is attributed to the different dissipation processes that occur:

(a) In glassy polymers, yield appears at low deformation and occurs near the crack tip in a domain of dimension r given by the linear model[1,2] $r_y \approx K^2/2\pi\sigma_y^2$, In this region the chains are oriented and form fibrils separated by microvoids (crazes). During crack propagation the sharp form of the tip does not change conspicuously.

(b) In elastomers, the applied deformations before rupture can be on the order of 10−100 higher; such materials violate both the requirement of Hookean behavior and small deformations which are embodied in the classical theory. In crystallizable elastomers, the round form of the tip change and becomes flat during deformation and the crack does not propagate up to rupture which can appear for high draw ratio $\lambda \approx 10$.

Stress-induced crystallization (SIC) in natural and synthetic elastomers have been studied experimentally[6−14] and theoretically[15−18] in detail by various authors. Gent et al.[13] concluded that the high tensile strength and crack growth resistance of natural rubber (NR) are due to its ability to crystallize (SIC). Andrews[8] has studied by birefringence the stress field around a crack in a rubber at low stress. By their technique they were not able to measure the crystallinity near the crack tip. Lee and Donovan[20] have studied the microstructural changes in the crack tip region of carbon black filled natural rubber. They verified that stress-induced crystallization occurs at the crack tip and measured the extent of the crystalline zone only along the symmetry axis of the crack perpendicular to the applied stress.

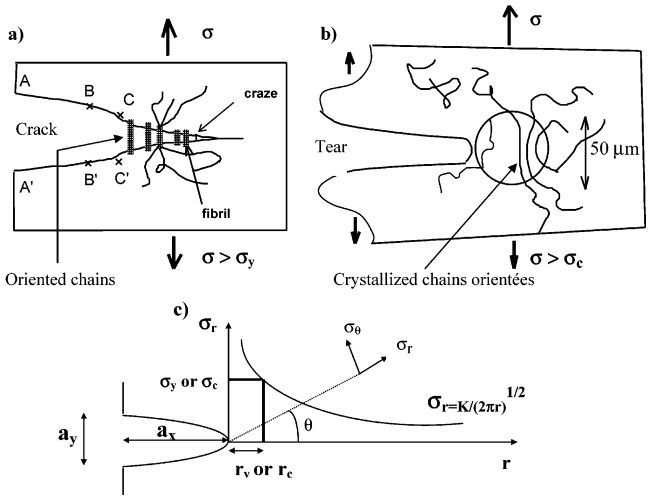

Figure 1. (a, b) Chain deformation around crack tips in amorphous (crazing) polymers and elastomers which show the stress-induced crystallization phenomena. (c) Distribution of the stress around a crack, in the case of small and elastic deformation. When the stress becomes equal to a critical value (σ_y: yield stress in amorphous solids, or σ_c the stress for inducing crystallization in elastomers) a zone of dimension r_c with different chain orientation is formed around the crack tip.

The differences and similarities of the deformed regions around crack tip in amorphous materials and elastomers are sketched in Figure 1. The aim of this work is to analyze in detail by X-ray diffraction the crystalline and relaxed regions found around the crack tip in a pure natural rubber material.

10.1021/ma021106c CCC: $22.00
Published on Web 12/04/2002

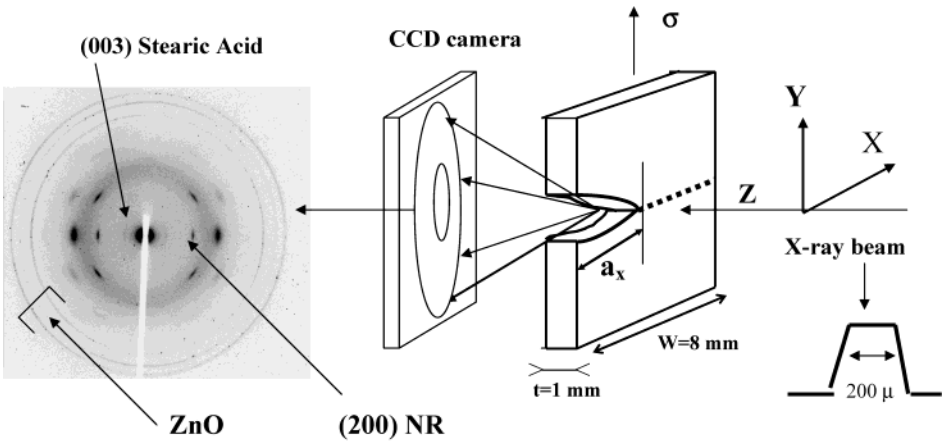

Figure 2. Experimental setup and typical X-ray diffraction pattern of NR having 5% zinc oxide and 2% stearic acid. The shape of the X-ray beam is indicated on the right side of the figure.

2. Experimental Procedure

The NR material presently used has the following composition for 100 g of *cis*-1,4-polyisoprene: sulfur, 1.2 g; stearic acid, 2 g; zinc oxide, 5 g; antioxidant, 1 g; accelerator, 0.8 g. Average cross-link densities $\nu \sim 6.2 \times 10^{-5}$ and 5.7×10^{-5} mol/g were estimated respectively by determination of the C_1 coefficient in the Mooney−Rivlin relation and by swelling measurements in toluene at room temperature. While some authors[7a] have found similar differences between the two methods, here we estimate that the difference can be explained by the accuracy of the measurements. The Young modulus at room-temperature deduced from the stress−strain curve at a strain rate $\dot{\epsilon} = 1\ s^{-1}$ is $E = 1.41$ MPa. At this strain rate, the engineering stress σ can be approximated by the linear relation in the range $2 < \lambda < 4.5$:

$$\sigma \approx 0.22 + 0.47\lambda \quad \text{(in MPa)} \tag{1}$$

The first set of experiments concerns the determination of the bulk material crystallinity as a function of draw ratio and temperature. For this purpose, samples having the form of a dumbbell were stretched by a drawing machine in an oven (temperature range: −30 to +100 °C) equipped with X-ray transparent Kapton windows. A tensile gauge enables one to follow the force during drawing or during heating experiments. The crack tip exploration was performed in a second set of experiments. A cut was made with a scalpel in the middle of samples; the sample is 30 mm long and 1 mm thick, and the width (8 mm) was chosen large in comparison to the cut length (in the range 0.5−1 mm). The sample was then stretched at room temperature and fixed on the $X-Y$ displacement stage (Figure 2).

Both experimental setups were mounted on a rotating anode generator equipped with homemade parallel beam optics (copper anode: $\lambda = 0.1542$ nm); a pinhole collimator reduced the beam diameter to ca. 0.2 mm (see beam profile in Figure 2). The beam-stop was chosen sufficiently small to allow the observation of some small-angle diffraction lines associated with crystallized stearic acid. The diffraction patterns were collected on a Princeton CCD camera with an exposure time of 3 min.

A typical diffraction diagram is displayed in Figure 2. The three larger angle reflection rings are due to zinc oxide crystals embedded into the sample. The crescent-like reflections correspond to highly oriented NR crystallites; the arc length is a measure of the degree of orientation of the crystallites with respect to the drawing direction. The diffuse halo originates from the NR amorphous fraction. The weak reflection at low angles corresponds to the (003) reflection of the crystallized stearic acid.

3. Experimental Results

3.1. Characteristics of Bulk NR. (a) Crystallinity. The crystallinity at room temperature has been determined by the two methods: Samples without cut have been drawn at room temperature, heated above 100 °C to erase their previous thermal history (as suggested by Flory[15]), and then rapidly cooled at constant length to −30 °C (samples A) or to room temperature, 22 °C (samples B). At −30 °C the kinetics of crystallization reaches a maximum rate;[7] at 22 °C crystallization is not observed for $1 < \lambda < 3$. These two types of samples were allowed to crystallize until no evolution of the diffraction pattern could be observed. The change in intensity of the (200) Bragg reflection of NR was then measured during slow warming-up; however, it is clear that the intensity I_{200} of this reflection depends on the variations in beam intensity, sample absorption and acquisition time. These corrections are taken into account if one considers the ratio I_{200}/I_{ZnO}, where I_{ZnO} is the integrated intensity of the three zinc oxide diffraction rings measured on the whole azimuthal angle range. Furthermore, this parameter allows a comparison between different NR samples as long as they have a similar zinc oxide content. This ratio can then be considered as an index of crystallinity.

In Figure 3a, the crystallinity index I_{200}/I_{ZnO} for samples A is given as a function of temperature in a heating experiment; measurements are done every $\Delta T = 4$ °C. The stabilization time Δt when the temperature is changed is about 20 min. During this time the tensile force stabilizes. Therefore, the equivalent heating rate is $q = \Delta T/\Delta t = 0.2$ °C/min for the various draw ratios. It is noted that at low temperature (−30 °C) this index I_{200}/I_{ZnO} is nearly constant. It has been found that samples B for $\lambda > 3$ have the same crystallinity index as samples A when heated above room temperature.

Also during this thermal treatment the scattered intensity of amorphous halo was recorded as a function of temperature. From the intensity $I^*_a(s)$ and $I_a(s)$ scattered respectively by the semicrystalline material at each temperature and by the completely amorphous material (just above T_m) one deduces the crystallinity $\chi = (I_a - I^*_a)/I_a 100$. Dumbleton et al.[19] and Lee et al.[20] used this method and showed that corrections due to the orientation does not change significantly the measurement of χ. From these measurements at different draw ratios λ, the correspondence between the crystallinity index $I_{200}(\lambda)/I_{ZnO}$ and the crystallinity χ (λ) is obtained at any temperature; this is reported in Figure 3a.

One draws the following conclusion: the crystallinity (and the crystallinity index) and the melting tempera-

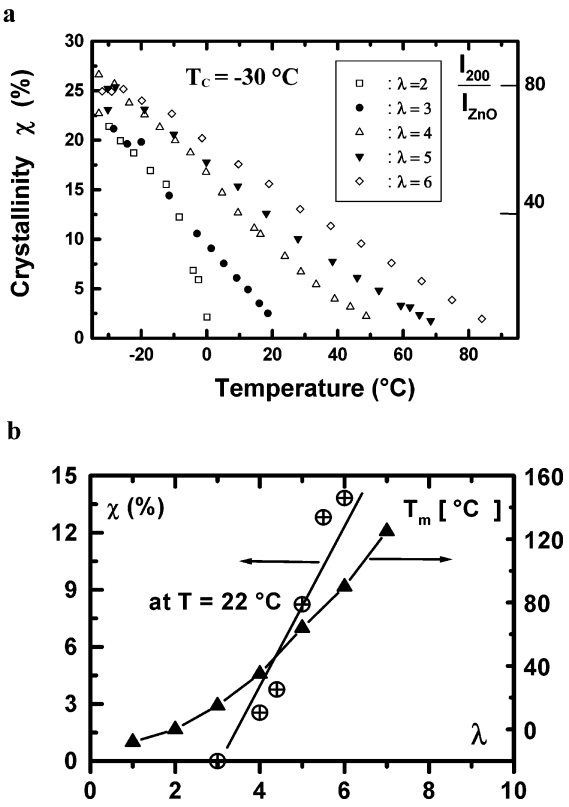

Figure 3. (a) Index of crystallinity I_{200}/I_{ZnO} of the NR deduced from the 200 reflection and crystallinity χ of NR as a function of temperature for five different draw ratios λ (samples A; equivalent heating rate: $q \sim 0.2$ °C/min, 20 min between two temperatures). (b) Crystallinity χ deduced from part a measured at room temperature as a function of λ. Melting temperature T_m deduced from part a by extrapolation of the crystallinity to zero.

ture do not depend on the previous thermal treatment. In Figure 3b the variation of χ at room-temperature deduced from Figure 3a is given. In this figure the melting temperature $T_m(\lambda)$ is also given, this temperature is obtained by extrapolating the crystallinity of Figure 3a to zero. The general behavior of $T_m(\lambda)$ is in good agreement with data published by Gent et al.[13] on different NR materials cross-linked with 1% dicumyl peroxide (of similar modulus), based on the measurement of the relaxation force. By X-ray measurements, Sietz et al.[9] found similar results for natural rubber. At room temperature, the critical draw ratio under which no stress-induced crystallization appears at room temperature is $\lambda_c \approx 3$.

(b) Orientation of the Amorphous Chains. Orientation of the amorphous chains of the sample is in general expected from an analysis of the diffuse halo (as shown in Figure 2) as shown by Mitchell,[21] Lee et al.,[20] and Murakami et al.[24] In NR as noted by Mitchell for scattering vector $\mathbf{s} = 1.35A^{-1}$, the observed anisotropy in the scattering is much less than the anisotropy in the molecular orientation. Also it must be noted that the rubber materials might possess some unoriented fraction of amorphous chains due to heterogeneity of cross-linking, this would contribute to the weak anisotropy of the amorphous halo. In our samples drawn at $\lambda = 4$, the amorphous orientation ratio $(I_E - I_M)/I_E$ (I_E and I_M being the equatorial and the meridian intensities of this diffuse halo) is weak and on the order of 5.2%; similar ratios 6.2% and 4% were observed, respectively, by Mitchell (Figure 2 of ref 21) and by Murakami et al. (Figure 4 of ref 24) for similar NR samples.

For low draw ratio, this method would be possible, but one proposes here an alternative method based on the analysis of the small-angle diffraction of the stearic acid added as cross-linking accelerator. A significant part of this fatty acid is crystallized as evidenced by the observation of specific diffraction lines in the small and wide angles regions (see Figure 2). The orientation of these crystallites appears to be highly sensitive to the elongation state of the surrounding polymer matrix. This feature can be explained by the plateletlike aspect usually exhibited by fatty acid crystals; an alignment of the normal to the lamellae perpendicular to the extension axis is observed. It must be noted that a similar method has been proposed by Lavebratt et al.[22] based on the orientation of zinc oxide crystallites. This method has not been used because the orientation of zinc oxide crystallites is isotropic. The lamellar periodicity of stearic acid (which has segregated during crystallization) is 5 nm, and the associated Bragg reflections are indexed as (00*l*). In the present experimental conditions, only the (003) reflection is detected (see Figure 2): the 10-times more intense (001) reflection remains hidden by the beam stop and the (002)is almost extinct. Because of the weakness of the reflection, we only have established a visual correspondence between the shape of the 003 reflection around the crack in our sample and in bulk samples drawn at different draw ratio, $1 < \lambda < 3$. In Figure 4c, the SA crystallites are more oriented (azimuthal angle ≈10−20°) at the border of the zone of maximum crystallinity than in the bulk (azimuthal angle ≈30−40°).

3.2. Crystalline Zones around the Crack Tip. (a) Contour Map of the Crystallinity Index. The following procedure has been applied for all the different draw ratios: (i) The shape of the crack is first determined by measuring the variation in the beam absorption as it crosses the sample border: the contour is represented by filled square symbols on the Figure 4a; the tip of the crack is taken as the origin. (ii) The diffraction patterns are then recorded by scanning the sample in the *X* and *Y* direction; each displacement is of the order 50 μm. It may be noticed that the crystallinity index I_{200}/I_{ZnO} is not sensitive to the beam fraction that actually crosses the sample and as noted above is not sensitive to the variation of thickness around the crack.

For example, the contour map of the crystallinity χ in the crack vicinity is given in Figure 4a for a sample drawn at $\lambda = 2.1$, the initial cut length is 1 mm. For more clarity, in the right side of this figure the scale of the *X* axis is 10 times that of the *Y* axis: the crystalline region is in fact flattened in the *Y* direction. Taking into account the calibration curve $\chi(\lambda)$ of Figure 3b each isocrystallinity curve corresponds to an isoextension curve; i.e., a place in the sample where the local draw ratio is constant. This isoextension map is given in Figure 4b, and the samples have been drawn at $\lambda = 2.1$; therefore, no stress-induced crystallization appears in the bulk (far from the crack tip).

Two distinct regions are distinguished in the crystalline deformed zone (CDZ) of Figure 4b: (a) Inside the crosshatched area, the degree of crystallinity remains constant. ($\chi_{max} \approx 12\%$.) The local draw ratio λ_{max} deduced from the calibration curve $\chi(\lambda)$ is in the range $5.5 < \lambda_{max} < 6$]. (b) A transition zone acts as a buffer between this

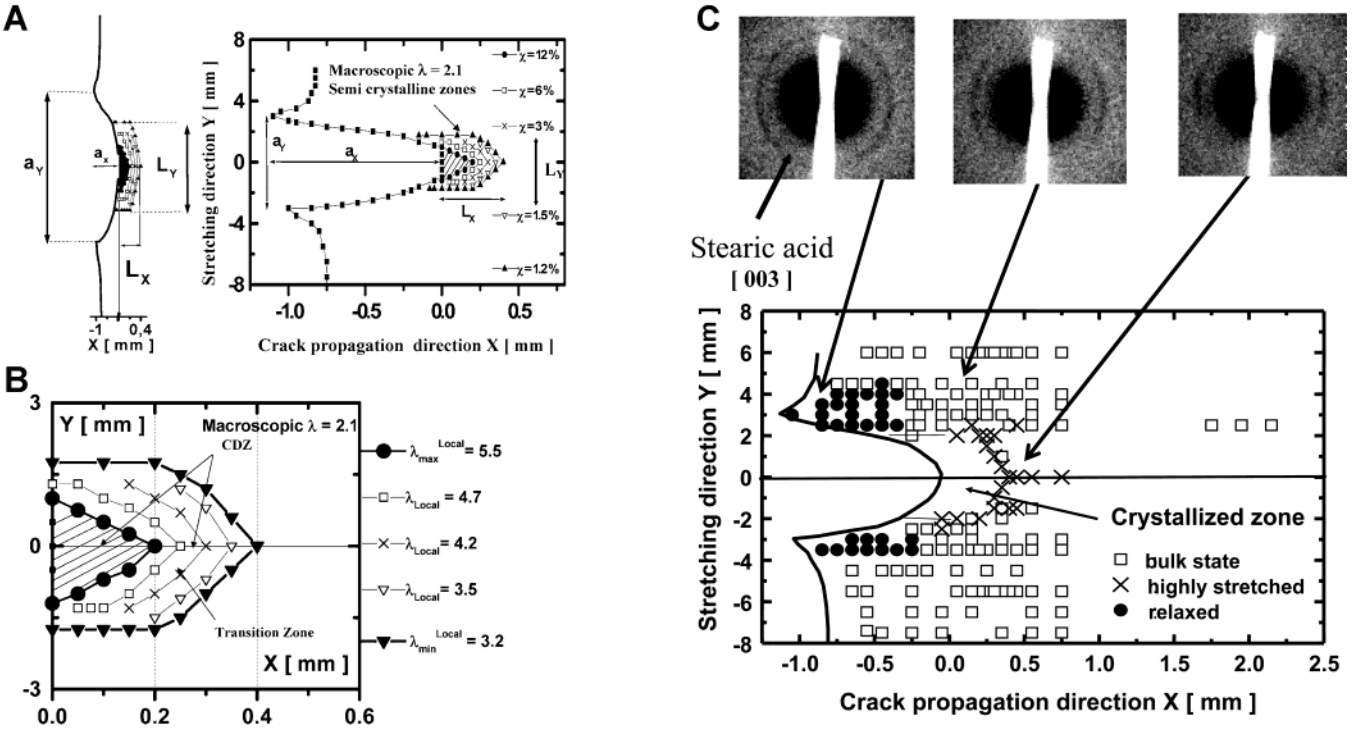

Figure 4. Deformed crystalline zones in a NR sample (initial sample width 8 mm, crack length $a_X = 1$ mm, and macroscopic draw ratio $\lambda = 2.1$: (a) Isocrystallinity contour map around the crack tip. The scale of the X and Y axis are the same on the left drawing and different on the right drawing. (b) Iso-local-draw-ratio contour map deduced from part a using the calibration curve $\chi(\lambda)$ of Figure 3b. (c) Orientation of the (003) reflection of stearic acid crystallites in the bulk (squares), deformed crystalline zone (cross), and the relaxed region (plain circles).

highly crystallized zone and the oriented amorphous bulk material. In the transition region, the crystallinity (and therefore the local draw ratio) decrease continuously with increasing distance r from the crack tip: linearly along the stretching direction OY (Figure 5a) and more rapidly along the transverse direction OX (Figure 5b). The minimum crystallinity that can be detected is $\chi_{min} \approx 1.2\%$, and this corresponds to a draw ratio $\lambda = 3.2$.

In view of the semiquantitative aspect of these results, no beam-size deconvolution is performed; computer simulations show that the extension of the zone of maximum crystallinity is underestimated by typically 0.05−0.1 mm, whereas the transition zones dimensions remains almost unaffected. The deconvolution does not change the linear aspect of the evolution of χ along the stretching direction (Figure 5a), the beam size being 10 times less than the width of the CDZ. In the case of Figure 5b, deconvolution brings about a steeper variation of the crystallinity χ along the OX direction.

These results are somewhat different from those obtained by Lee et al. on similar NR (but as noted above of different modulus and crystallizing at $\lambda = 2$ in the bulk state at 22 °C). Along the OX direction they observed a decrease of the crystallinity on the form $\chi = 1/r$ but they do not find the plateau of crystallinity near the crack tip. This probably is due to the size of the X-ray beam (0.3 mm instead of 0.2 mm in this work) and/or to the fact that the scan is not perfectly along the symmetry axis OX. In Figure 5b, it is demonstrated that at a distance $y = 0.5$ mm above or below the OX crack axis, the plateau length is decreased by a factor two.

(b) Orientation of the Crystalline Chains. The crescentlike aspect of the (200) Bragg reflection indicates the preferential orientation of the NR crystallites

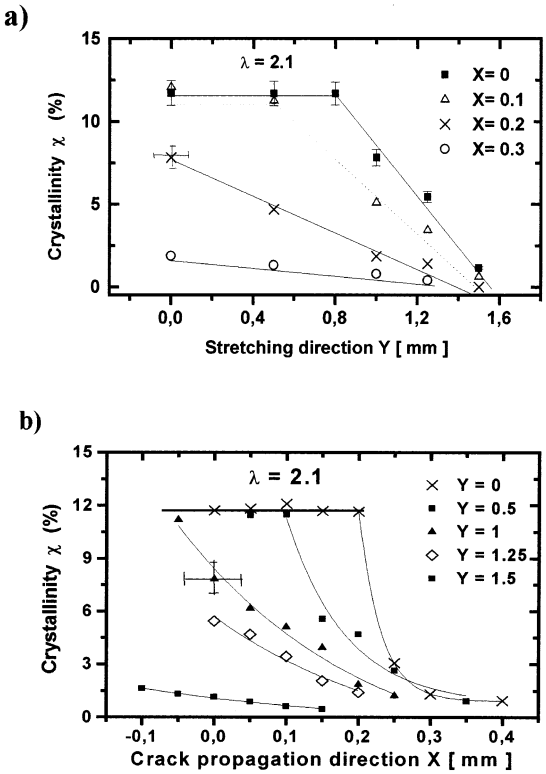

Figure 5. Crystallinity χ near the crack tip as a function of the distance from the origin along the directions X(**a**) and Y(**b**) for respectively different positions y (a) and x (b). NR sample of Figure 4.

in the drawing direction. The azimuthal width at half intensity $\Delta\psi_{1/2}$ is a measure the deviation from this direction. The variation of the azimuthal width $\Delta\psi_{1/2}$ of the (200) NR reflection along the X axis is reported

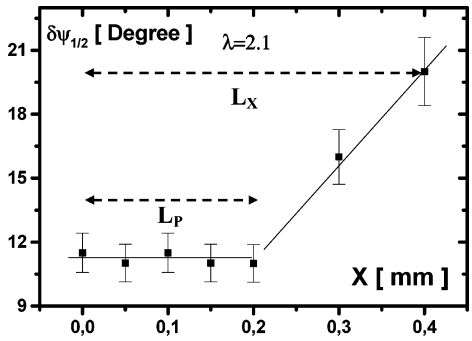

Figure 6. Variation of the azimuthal angle $\Delta\psi_{1/2}$ of the 200 reflection of the NR crystallites vs the distance x along the OX axis (sample of Figure 4). The NR sample has been drawn at $\lambda = 2.1$, the crack length is $a_X = 1$ mm. Near the crack tip, the azimuthal angle 12° at the plateau is equal to the minimum value obtained in bulk rubber stretched beyond $\lambda = 5$ at room temperature.

in Figure 6 for the same sample drawn at $\lambda = 2.1$. In the zone of maximum crystallinity, $\Delta\psi_{1/2}$ remains constant. Its value of 11.5° is close to the azimuthal angle observed in bulk samples for λ in the range $4 < \lambda < 6$ (then in crystallized samples, see Figure 3b). Similar values in bulk NR has been reported by Gaylord.[17]

In the transition zone, $\Delta\psi_{1/2}$ increases gradually up to 20° which indicates a slight loss of crystallite orientation.

3.3. Relaxed Zone near the Crack Tip. A new effect, unobserved in amorphous polymers, arises in NR samples drawn at low ratio $\lambda < 3$. During deformation the width of the dumbbell far from the crack varies obviously according to the affine model ($\propto 1/\sqrt{\lambda}$); in fact, just above and below the crack surfaces the width of the sample does not change conspicuously. A bump is observed on the lateral surface, as shown in Figures 1b and 4a, that is expected to correspond to a completely relaxed zone; thus the local draw ratio in the zone surrounding the CDZ has been estimated using the (003) Bragg reflection of the stearic acid as explained above. In Figure 4c, one gives the shape of the stearic acid reflection in the three different regions around the crack. Far from the crack (squares), the reflection aspect qualitatively corresponds to what is expected for the bulk sample drawn at $\lambda = 2.1$. One stress here again that these lamellar crystallites in the bulk state are more oriented (Figure 4c) than the amorphous chains (Figure 2); due to the shape of the lamellae a small orientation of the amorphous chains induces an important orientation of these lamellae. Near the crystalline deformed zones (crosses), the arc length of the reflection is reduced ($\Delta\phi \sim 25-30°$); the same arc length refection is found in bulk NR drawn above $\lambda = 2.3$. In the bump region (plain circles) the (003) reflection is isotropic, this confirms that the NR chains are relaxed in this region. The measurement of the orientation of the fatty acid crystallites is not very accurate (the accuracy on the azimuthal angle is about 10−20°); however, the trend observed indicates clearly that the surface of the relaxed zone corresponds approximately to the opening surface of the cut.

3.4. Effect of the Draw Ratio λ on the Crystalline Zone Dimensions. Dimensions of the Deformed Region. Similar contour maps of the crystallinity χ have been obtained for different draw ratios. As shown in Figure 4a, we define respectively the crack and CDZ dimensions as respectively a_X, a_Y and L_X, L_Y. These

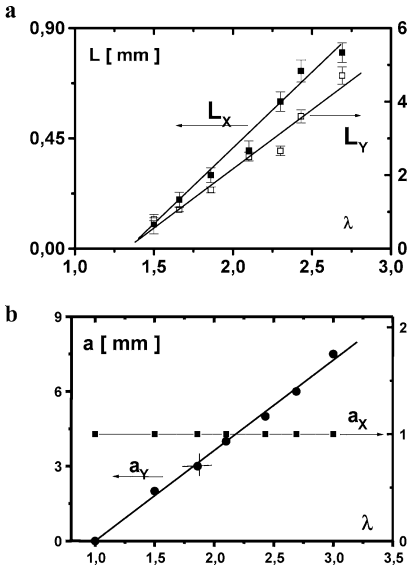

Figure 7. Dimensions of the crystalline deformed zones (CDZ) vs λ (sample of Figure 4). For $\lambda < 3.5$, stress-induced crystallization does not occur in the bulk; NR crack length $a_x = 1$ mm. (a) Dimension L_X and L_Y of the (CDZ) around the crack tip. (b) Dimensions a_X and a_Y of the COD (crack opening distance).

characteristic lengths are plotted in Figure 7 as a function of the macroscopic draw ratio λ. From these graphs, the following points are emphasized: (a) No crystallization at the crack tip is observable below $\lambda \approx 1.3$. Above this value, L_X and L_Y increase linearly until $\lambda \approx 2.7$; the CDZ area varies thus as λ^2. A dramatic increase (not represented in the figure) is observed above this value, which corresponds to the approach of the critical value $\lambda_c \approx 3$ where stress-induced crystallization appears in the bulk material at room temperature. It is interesting to compare these variations in $L_X(\lambda)$ to those reported by Lee et al. on pure and carbon-black-filled NR (Figure 6 of ref 20). These authors observed the dimensions of the crystalline zone at draw ratio $\lambda = 1.5$ and $\lambda = 2$ (for pure NR). The slope $dL_X/d\lambda$ deduced from these two measurements is about 0.3 mm and is equal to the slope observed in Figure 7a. The main difference between ours results and those reported by these authors is that in their case stress-induced crystallization occurs as soon as the NR is drawn and that the variation of $L_X(\lambda)$ is not linear below $\lambda = 1.5$. (b) The crack length a_X does not change during deformation. The crack opening distance a_Y and the CDZ vertical dimension L_Y are of the same order of magnitude and vary in the same way. The difference in the form of the crack tip between glassy (sharp) and crystallizable elastomer (flat, see drawing on left part of Figure 4a) materials is due to the stress-induced crystallization. Oriented crystallites formed in NR all along the flat border of the crack impede the fracture propagation.

3.5. Effect of the Crack Depth on the Crystalline Zone Dimensions. The Inglis model for amorphous polymers predicts that yield occurs near the crack tip in a domain of dimension $r_y \approx K^2/2\pi\sigma_y^2$, where $K = \sigma_0\sqrt{\pi a}$ is the stress intensity factor, σ_0 the applied stress, and a the crack length (see above). By analogy, one expects the CDZ extension to vary similarly with the crack length. Figure 8 compares the CDZ dimensions of samples drawn at $\lambda = 2.1$, with cut lengths 0.5 mm (a) and 1 mm (same as in Figure 4). In the figure

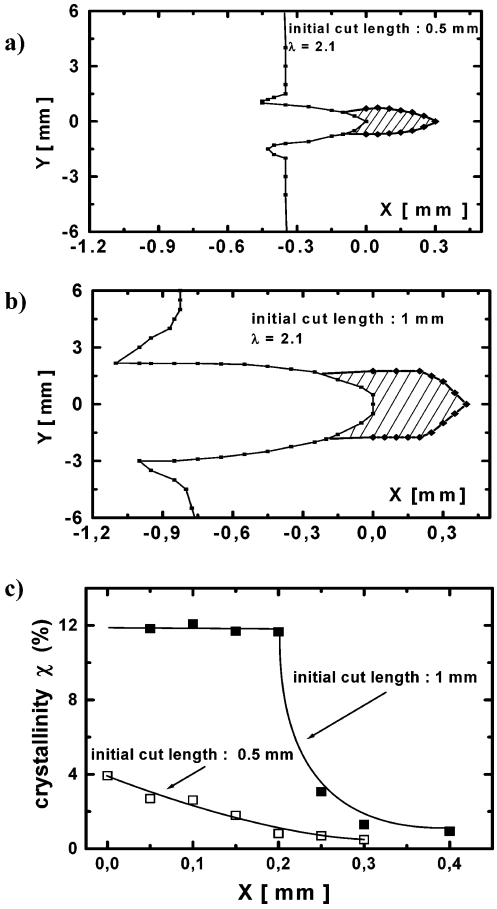

Figure 8. (a, b) Dimensions of the crystalline deformed zones (CDZ) in NR with crack length $a_X = 0.5$ mm (a) and 1 mm (b). (c) Crystallinity χ vs the distance x from the crack tip along the X axis, for the two samples a and b.

the limits of the crystallized zones (hatched area) are indicated, plain circles correspond to the minimum of crystallinity ($\chi \approx 1.2\%$), which can be detected. In case a, the CDZ dimension L_y is reduced by a factor of 2 compared to case b. The dimension L_x does not vary conspicuously.

In Figure 8c, the crystallinity along the Ox axis is given for both cases. In the case of small cut the crystallinity decreases continuously and no plateau is observed. One concludes that for a constant draw ratio the observation of a crystallinity plateau require a critical cut length and therefore a critical local draw ratio (as suggested by the relation $\sigma_y \approx \sqrt{a}$).

In conclusion, when the draw ratio or the crack length are changed, the CDZ dimensions in the stretching direction and the crack opening distance vary in the same way.

3.6. Variation of Local Stress with the Distance. Crack Tip Axis. Figure 9a gives the variation of the crystallinity χ along the crack axis ($y = 0$) in the CDZ for several draw ratios for a cut length $a_x = 1$ mm. One concludes that at constant cut length a crystallinity plateau ($\chi = 12\%$) is observed when the macroscopic draw ratio is higher than 2; this indicates that the local draw ratio reaches the critical value $\lambda = 5.5$ (Figure 3b shows that when $\chi = 12\%$ the draw ratio is $\lambda = 5-6$).

In Figure 9b, one has redrawn the crystallinity curve corresponding to $\lambda = 2.43$ (the corresponding macroscopic stress is $\sigma_0 = 0.9$ M Pa), then using relationship

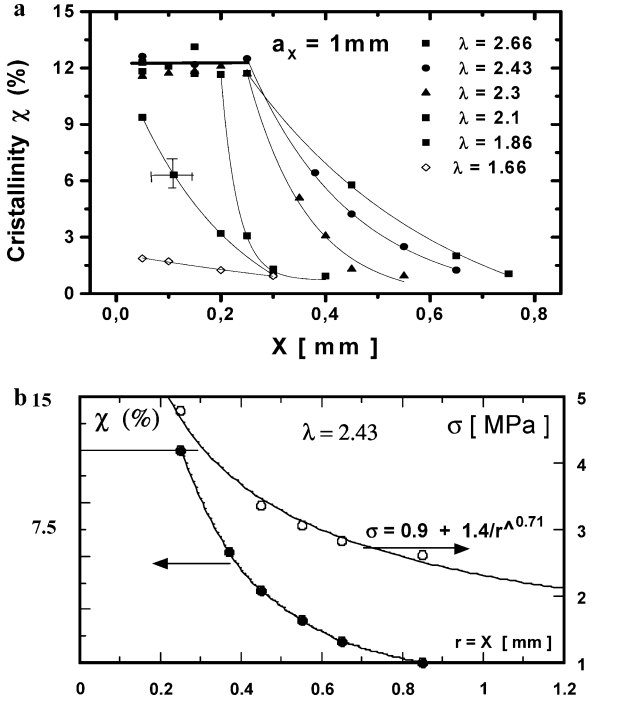

Figure 9. (a) Crystallinity χ as a function of the distance x along the crack axis for various draw ratio, NR initial sample width 8 mm, crack length $a_X = 1$ mm. (b) Crystallinity χ (plain triangle) and stress component $\sigma = \sigma_{yy}$ (open triangle) along the OX axis for the sample of Figure a drawn at $\lambda = 2.43$ The local stress σ is deduced from the local draw ratio λ_l (relationship 1) given by the calibration curve $\chi(\lambda_l)$ of Figure 3b. The line is the best fit with the power law $\sigma \sim 1/x^{0.7}$ (relationship 2, see Table 1).

1 the local stress $\sigma(x)$ is plotted. For this value of λ, the transition zone is 4 times the beam size, and therefore, the deconvolution effect can be neglected.

In the linear and nonlinear (hyperelastic) elasticity models, the stress components depend differently on the polar coordinates. In the linear theory,[1] assuming plane stress and incompressibility conditions, the component σ_{yy} parallel to the draw direction is given by the relation $\sigma_{yy} \approx \sigma_0(a/r)^{1/2}$. Here to recover the value $\sigma_{yy} = \sigma_0$ for $r > a$, one writes:

$$\sigma_{yy} = \sigma(r) = \sigma_0 + \sigma_1(a/x)^n \qquad (2)$$

The stress σ_1 is considered here as a fitting parameter. Same variation is expected for the Oy direction. In the linear theory the exponent is $n = 0.5$. In the Neo-Hookean[2,3] and Stephenson,[4] models based on the first ($N = 1$) and third order ($N = 3$) expansion of the Rivlin constitutive law, the exponent is $n = 1$. The first term σ_0 is the applied stress (σ value far from the crack tip); it is generally dropped when $\sigma(r) > \sigma_0$, but this is not the case here. One gives in the following table the fit parameters with these two types of models.

In the linear model, the fit is bad, the correlation factor is $R = 0.94$, and the value of the parameter $\sigma_1 = 2.3$ MPa is far from the applied stress $\sigma_0 = 0.7$ MPa. The best fit is found for $n = 0.7$ the fit curve passing through the experimental points in the figure obeys the relation $\sigma(r) = 0.9 + 1.4/r^{0.7}$, the exponent $n = 0.7$ is intermediate between the value $n = 0.5$ of the linear model, and the value, $n = 1$, of the hyperelastic models. The behavior of the crystallinity along the crack axis cannot be explained by the linear and hyperelastic theories.

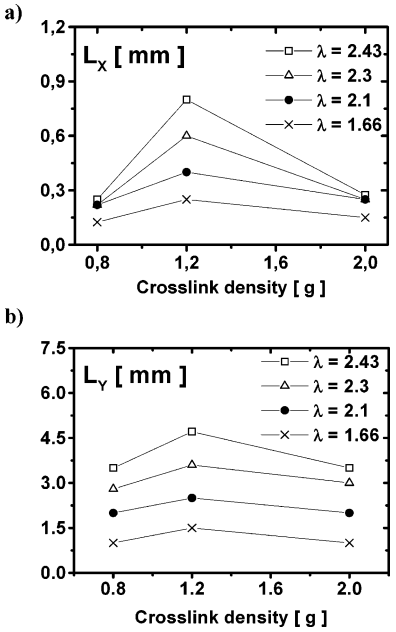

Figure 10. Dimensions L_X (a) and L_Y (b) of the crystalline deformed zones (CDZ) around the crack tip in NR as a function of the cross-link density for different draw ratio. The cut length is $a_x = 1$ mm.

Stretching Direction. From Figure 5 and using relelationships 2 and 3, it is clear that the form of the $\sigma(r)$ curve in the transition zone is linear along the *Oy* direction at any *x* value; this is not predicted either by the Inglis model or by the hyperelastic models. In each model the components σ_{yy} along the two directions *Ox* and *Oy* are given by the same scaling law $\sigma_{yy} \sim 1/r^n$. Again here one stresses that the trapezoidal shape of the X-ray beam cannot explain the different variations of σ along the *X* and *Y* axis.

In conclusion, the linear and the hyperelasticity models cannot explain the distribution of the stress around the crack tip. This is not surprising because the crystallization process changes the local stress field.

We suggest that the difference in the scaling laws $\sigma_{yy} \approx -r$ and $\sigma_{yy} \approx 1/r^{0.7}$ observed in the two perpendicular directions is due to the relaxation of the local stress (in the direction of stretching) when crystallization occurs; this effect of stress relaxation during crystallization is well-known in bulk crystallizable elastomers[7,15] and in gels of polyethylene.[24] In our bulk sample drawn at $\lambda = 5$ (without crack), the macroscopic stress relaxes by 20% during crystallization, and similar values have been reported in the literature.[7a,15] Unfortunately, there is no method which permits one to measure directly this local stress in such small zones.

3.7. Variation of the Crystalline Zone Dimensions with the Cross-Linking. The same procedure has been applied to NR samples cross-linked with 0.8 and 2 g of sulfur with the same concentration of accelerator. In the following table, one gives the characteristics of these three types of rubber the modulus and degree of cross-linking are compare to the preceding sample (1.2 g of sulfur).

One reports in Figure 10 the dimensions L_X and L_Y of the crystalline zones as a function of the cross-link density (in grams of sulfur) for various draw ratios. The crystalline zones for each draw ratio are larger for the medium value of cross-linking (1.2 g), indicating that the dimensions would have a maximum value for sulfur concentration between 0.8 and 2 g. In Table 2 one remarks that the tensile strength pass also by a maximum in the same domain of cross-link density. Hamed[25] reported that tear and tensile strength of rubbers pass trough a maximum as cross-linking increases indicating that the optimum of cross-links for practical use must be high enough to prevent failure by viscous flow but low enough to avoid brittle fracture, this author reported that the cross-link densities corresponding to the maximum of the tear and tensile strengths could be different. In the tearing geometry adopted in this work, one concludes that deformations during tearing and drawing involve the same microscopic process (stress-induced crystallization and chains breakage at the rupture) and therefore the same dissipation phenomena.

Table 1. Best Fit Parameters of Relationship 4 for NR Sample Drawn at $\lambda = 2.44$ (*R* Correlation Factor)

$\sigma(r) = \sigma_1/r^n$; $r = x$	$\sigma_1 = 2.3$ MPa	$n = 0.5$	$R = 0.993$
$\sigma(\rho) = \sigma_0 + \sigma_1/r^n$; $r = x$	$\sigma_1 = 1.4$ MPa	$n = 0.7$	$R = 0.997$
	$\sigma_1 = 1.7$ MPa	$n = 0.5$	$R = 0.94$

Table 2. Relation between Cross-Linking Density and Mechanical Properties of the Pure Rubbers

mass of sulfur in 100 g NR, g	0.8	1.2	2
Young modulus E, MPa	1.08	1.41	2.4
cross-link density ν, mol/g	4×10^{-5}	5.7×10^{-5}	9.4×10^{-5}
stress at break σ_b, M Pa	8.2	10.4	11.3
tensile strength, 10^6 J/m^3	2.01	2.6	2.34

4. Conclusion

The dimensions and morphology of the crystalline deformed region in all the space around the crack tip in drawn NR samples has been determined with a good accuracy by X-rays diffraction using a simple X-ray laboratory source. The most important results obtained on NR samples with crack length 1 and 0.5 mm can be summarized as follows:

(i) A crystallized zone (CDZ) appears at the tip of the crack at draw ratios as low as $\lambda = 1.3$.

(ii) The dimension of the CDZ along the draw direction L_Y increases linearly with λ and is close to the crack opening distance, a_Y.

(iii) The dimension of the CDZ along the transverse direction L_x also increases linearly with λ but remains approximately 10 times lower than L_Y; the area of the CDZ varies then as λ^2.

(iv) The dimension L_y of the CDZ depend on the initial cut length; a 2-fold increase has been observed when doubling the cut length. The L_x dimension does not seem to change with the cut length.

(*v*) Increasing the cut length is equivalent to increasing the draw ratio (compare Figures 8c and 9a)

(vi) An analysis of the CDZ reveals a highly crystalline zone where the crystallinity and the crystallite orientation remain constant ($\chi \approx 12\%$, $\Delta\psi_{1/2} \approx 11°$) the width of the transition region between the bulk and this highly crystalline zone depends on the draw ratio.

(vii) The component σ_{yy} of the local stress along the crack tip axis in the transition zone verifies the scaling law $\sigma(r) \approx \sigma_1/r^n$, the exponent varies with the draw ratio. For $\lambda \approx 2.4$, the exponent *n* is intermediate between the predictions of the linear theory and the hyperelastic model (Figure 9b). A better accuracy on the scaling exponent would require a deconvolution procedure or/ and a smaller X−ray beam size.

(viii) A completely relaxed zone is found between the border of the sample and the crack tip; this effect produces a bump outside the crack opening surfaces. This state of relaxation is confirmed by a measure of the orientation of stearic acid crystallites embedded into the elastomer matrix; the area of this region is close to the crack opening surface and of the area of the CDZ.

(ix) The CDZ dimensions present a maximum for a concentration of sulfur between 0.8 and 2 g of sulfur per 100 g of NR. The fact that the tensile strength and the CDZ dimensions pass through a maximum for the same density of cross-links indicates clearly that the processes of deformation in the crack tip and in the bulk are the same. The formation of the plateau of crystallinity is the essential process which permits the dissipation (absence of diverging stress when $r \rightarrow 0$ and consequently absence of rupture of the chains near the crack), the maximum local stress suggested by the existence of this plateau is much smaller than the breaking stress σ_b.

With our experimental setup, one was able to measure the crystallinity in a very small zone of width 0.05 mm at the border of the crack tip. For low extension $\lambda < 1.8$, no plateau of the crystallinity (Figure 9a) is observed, and one must wonder if this is an intrinsic effect of the material suggested by the observed variations of the crack dimensions L_x and L_y with λ (Figure 7a) or due to the size of the X-ray beam. This feature must be analyzed in detail using the same technique with a microbeam at a synchrotron source.

Acknowledgment. We want to thank Dr. P. Johnson and M. Favrot from Michelin Co. for stimulating discussions and remarks about this work

References and Notes

(1) Kausch, H. H. *Polymer fracture*; Springer-Verlag: Berlin, 1987.
(2) Liebowitz, H. *Fracture*; Academic Press: New York, 1992.
(3) Quigley, C. J.; Parks, D. M. *Int. J. Fract.* **1994**, *65*, 75.
(4) Stephenson, R. *J. Elasticity* **1982**, *12*, 65.
(5) Kwoles, J. K.; Sternberg, E. *J. Elasticity* **1983**, *13*, 257.
(6) Thomas, A. G. *J. Polym. Sci.* **1955**, *18*, 177.
(7) (a) Gent, A. N. *Trans. Faraday Soc.* **1954**, *50*, 521. (b) Gent, A. N. In *Engineering with Rubber*; Hanser Publishers: Oxford University Press: Oxford, England, 1992.
(8) Andrews, E. H. *Proc. Phys. Soc.* **1961**, *77*, 483.
(9) Sietz, W.; Goritz, D.; Muller, F. H. *Colloid Polym. Sci.* **1974**, *262*, 854.
(10) Hamed, G. *Rubber Chem. Technol.* **1990**, *64*, 493.
(11) Lake, G. L. J.; Samsuri, A.; Teo, S. C.; Vaja, J. *Polymer* **1991**, *32*, 2963.
(12) Hamed, G. R.; Kim, H. J.; Gent, A. N. *Rubber Chem. Technol.* **1996**, *69*, 807.
(13) Gent, A. N.; Kawahara, S.; Zhao, J. *Rubber Chem. Technol.* **1998**, *71*, 668.
(14) Magill, J. H. *Rubber Chem. Technol.* **1995**, *68*, 507.
(15) Flory, P. J. *J. Chem. Phys.* **1947**, *15*, 397.
(16) Krigbaum, W. R.; Roe, R. J. *J. Polym. Sci.* **1964**, *A2*, 4391.
(17) Gaylord, R. J. *Polym. Lett. Ed.* **1975**, *13*, 337; *J. Polym. Sci. (Polym. Phys. Ed.)* **1976**, *14*, 1827.
(18) Smith, J. *Polym. Eng. Sci.* **1976**, *16*, 168.
(19) Dumbleton, H.; Bowles, B. B. *J. Polym. Sci. (Part A2)* **1966**, *4*, 951.
(20) Lee, D. J.; Donovan, J. A. *Rubber Chem. Technol.* **1987**, *60*, 910.
(21) Mitchell, G. R. *Polymer* **1984**, *25*, 1562K.
(22) Lavebratt, H.; Stenberg, B.; Werner, P.-E. *Polymer* **1993**, *34*, 1109.
(23) Posthuma, A.; De Boer Pennings, A. J. *Faraday Discuss., Chem. Soc.* **1979**, *345*, 68.
(24) Murakami, S.; Senoo, K.; Toki, S.; Kohjihya, S, *Polymer* **2002**, *43*, 2117.
(25) Hamed, G. R. In Ref 7b, Chapter 2, p 11.

MA021106C